A sinuous tumulus over an active lava tube at Kīlauea Volcano: evolution, analogs, and hazard forecasts

Tim R. Orr[1,2,*], Jacob E. Bleacher[3], Matthew R. Patrick[1], Kelly M. Wooten[1,4]

[1]*Hawaiian Volcano Observatory, U.S. Geological Survey, Hawaii National Park, HI 96718*

[2]*Department of Geology and Geophysics, University of Hawaii, Honolulu, HI 96822*

[3]*Planetary Geodynamics Laboratory, NASA Goddard Space Flight Center, Greenbelt, MD 20771*

[4]*Department of Geological and Mining Engineering and Sciences, Michigan Technological University, Houghton, MI 49931*

[*]*Corresponding author. Tel.: +1-808-967-7328; E-mail address: torr@usgs.gov*

Abstract

Inflation of narrow tube-fed basaltic lava flows (tens of meters across), such as those confined by topography, can be focused predominantly along the roof of a lava tube. This can lead to the development of an unusually long tumulus, its shape matching the sinuosity of the underlying lava tube. Such a situation occurred during Kīlauea Volcano's (Hawai'i, USA) ongoing East Rift Zone eruption on a lava tube active from July through November 2010. Short-lived breakouts from the tube buried the flanks of the sinuous, ridge-like tumulus, while the tumulus crest, its surface composed of lava formed very early in the flow's emplacement history, remained poised above the surrounding younger flows. At least several of these breakouts resulted in irrecoverable uplift of the tube roof. Confined sections of the prehistoric Carrizozo and McCartys flows (New Mexico, USA) display similar sinuous, ridge-like features with comparable surface age relationships. We contend that these distinct features formed in a fashion equivalent to that of the sinuous tumulus that formed at Kīlauea in 2010. Moreover, these sinuous tumuli may be analogs for some sinuous ridges evident in orbital images of the Tharsis volcanic province on Mars. The short-lived breakouts from the sinuous tumulus at Kīlauea were caused by surges in discharge through the lava tube, in response to cycles of deflation and inflation (DI events) at Kīlauea's summit. The correlation between DI events and subsequent breakouts aided in lava flow forecasting. Breakouts from the sinuous tumulus advanced repeatedly toward the sparsely populated Kalapana Gardens subdivision, destroying two homes and threatening others. Hazard assessments, including flow occurrence and advance forecasts, were relayed regularly to the Hawai'i County Civil Defense to aid their lava flow hazard mitigation efforts while this lava tube was active.

Keywords
Hawaii; New Mexico; Mars; Kilauea; flow inflation; lava tube; volcanic hazards

1. Introduction

Pāhoehoe flow fields emplaced on low-slopes (<~2º) commonly thicken endogenously via flow inflation (Nichols, 1939; Wentworth and Macdonald, 1953; Walker, 1991; Chitwood, 1994; Peterson et al., 1994; Hon et al., 1994; Cashman and Kauahikaua, 1997; Kauahikaua et al., 1998; Self et al., 1998; Anderson et al., 1999; Anderson et al., 2005; Walker, 2009; Anderson et al., 2012; Hoblitt et al., 2012) and are usually broad because flow advancement is generally accompanied by considerable flow widening. As inflation progresses, the upper surface of the flow lifts, and the separation between individual flow lobes vanishes, forming a molten core of interconnected pathways within the flow (Hon et al., 1994; Kauahikaua et al., 1998; Self et al., 1998; Anderson et al., 1999; Schaefer and Kattenhorn, 2004; Anderson et al., 2005; Anderson et al., 2012; Hoblitt et al., 2012). Inflation broadly affects the entire flow because of this hydraulic connection. The result is a flat to hummocky flow surface bounded by steep, rifted margins.

Hummocky flow surfaces are characterized by the presence of tumuli—low, dome-like mounds, commonly 1–5 m high, but occasionally exceeding 10 m in height (e.g., Wentworth and Macdonald, 1953; Walker, 1991; Chitwood, 1994). Most tumuli are crudely circular to elliptical in map view with deep axial cracks (e.g., Walker, 1991) and form in response to magmatic overpressure within the flow as the flow's crust thickens (Walker, 1991; Hon et al., 1994; Peterson et al., 1994; Anderson et al., 1999; Anderson et al., 2012). Those areas that inflate the most form tumuli, while the lows between tumuli experience significantly less, or even no, inflation. In practice, all low mounds that define the surface of hummocky flows, and which formed by inflation, are called tumuli.

In some instances, inflation is focused over preferred pathways, such as incipient tubes, within a flow to form a discontinuous series of elongate tumuli (Kauahikaua et al., 1998; Glaze et al., 2005). Such chains of tumuli can also form when pāhoehoe lava on a low-slope surface fails to spread out, for instance by lateral topographic confinement (Glaze et al., 2005). In this case, the geometry of the flow alone focuses inflation within the flow's narrow width, so that tumuli appear to be aligned. While the formation of a series of tumuli over a well-established lava tube occurs relatively rarely (Walker, 1991; Anderson et al., 2012), such occurrences have been documented (Kauahikaua et al., 1998; Duncan et al., 2004). Where tumuli form over such lava tubes, they tend to be more elongate, sometimes with a sinuosity that matches that of the underlying lava tube (Keszthelyi and Pieri, 1993; Hon et al., 1994; Cashman and Kauahikaua, 1997; Self et al., 1998).

In July 2010, during Kīlauea Volcano's (Hawai'i) long-lived East Rift Zone eruption, a new lava flow reached the gently sloping southeast coast and encroached on homes within the Kalapana Gardens subdivision (Figs. 1 and 2), near the village of Kalapana. As the flow traveled across the coastal plain, it was confined by gentle topography that prevented significant spreading. A master lava tube developed quickly, and the roof of the tube evolved into a ~1-km-long, 10- to 20-m-wide sinuous tumulus (Figs. 3 and 4). The tumulus grew gradually by flow inflation, but its development was punctuated by frequent breakouts from its flanks that slowly buried the tumulus and caused abrupt, irrecoverable uplift of its top. These breakouts occurred in response to recurring pressure fluctuations caused by cycles of deflation and inflation (DI events) at Kīlauea's summit (Fig. 5; Cervelli and Miklius, 2003; Poland et al., 2011), which were transmitted through the East Rift Zone to the eruption site and manifested as days-long fluctuations

in vent discharge. Inflation in this latter context refers to deformation of the volcanic edifice and is different from superficial flow inflation.

We focus here on the development of the very long, sinuous tumulus described above and discuss the hazards posed by the breakouts that occurred in response to fluctuations in discharge. The lava tube breakouts, when they occurred, started about a day after the onset of edifice inflation during the DI events. This timing provided a means of forecasting breakouts that subsequently threatened Kalapana Gardens.

The appearance of the sinuous tumulus that formed along the tube at Kīlauea during July–November 2010, and the gradual inundation of the tumulus by its own breakouts, created unusual flow field morphology. This tumulus may be analogous to similar features preserved within topographically confined areas of the prehistoric McCartys and Carrizozo flow fields (New Mexico, USA), as well as in the Tharsis volcanic province of Mars. Understanding how the inflated lava tube formed provides constraints on emplacement conditions in these other environments.

2. Eruption monitoring methods

2.1 Flow field mapping

Lava flow hazard assessments were conducted on almost a daily basis during the study period because of the proximity of lava flows to Kalapana Gardens. We mapped the margins of the active flows simply by walking around each flow while recording a track log with a handheld Global Positioning System (GPS) device. While time-consuming, this gave us a simple way to measure flow progress and to gauge other flow properties such as vigor, flow inflation, and potential flow paths. The flow's advance rate was very slow and therefore of little immediate concern. The initial western edge of the flow as it advanced across the coastal plain was not mapped on the ground due to time constraints, nor was most of the perimeter of the August 2, 2010, breakout, which is described below. The flow edges in these cases were approximated from oblique aerial photographs taken during weekly helicopter observation flights. The mapping was compiled using ESRI® ArcGIS software. Updated flow maps, accompanied by a descriptive hazard assessment, were then transmitted via email to Hawai'i County Civil Defense (HCCD; the agency charged with disaster preparedness and response on the Island of Hawai'i) on a near-daily basis. More immediate hazards-related concerns, when present, were transmitted directly to the HCCD administrator via text message.

2.2 Webcams and time-lapse cameras

Webcams and time-lapse cameras have long played a role at Kīlauea and are now among the standard tools used by many groups, including the United States Geological Survey's Hawaiian Volcano Observatory (HVO), to monitor and study eruptive activity (e.g., Thornber, 1997; Poland et al., 2008; Paskievitch et al., 2010; Orr, 2011). During the activity described here, two webcams provided images (1296 × 960) of the coastal flow field in real-time. Both were Stardot® Netcam SC webcams which transmitted images via the Verizon® cell phone network using an Airlink® Raven XE cellular modem. One camera was positioned on the second-floor patio of a house in Kalapana Gardens roughly 1.6 km from the sinuous tumulus. It operated almost continuously starting on September 18, 2010, and archived an image at HVO automatically every 30 minutes. The other webcam was positioned on Pūlama Pali, the 300-m-high slope overlooking the coastal flow field near Kalapana Gardens (Pūlama Pali is the common-usage name for this prominent slope, for which an official name has not been designated by the United

States Board on Geographic Names), roughly 1.1 km from the sinuous tumulus. It began operation on November 9, 2010, and an image was archived at HVO every 5 minutes. The webcams were programmed to automatically switch to a near-IR mode in low-light conditions. The images produced by the webcams were useful in determining the onset times of many of the breakouts, particularly those that occurred at night when the near-IR mode was functioning.

As many as six time-lapse cameras were deployed simultaneously along the crest of the sinuous tumulus, or adjacent to it, during the study period, specifically to document the evolution of the tumulus that we describe in this paper. The cameras were of two types—low-cost Wingscapes® time-lapse cameras mounted on inexpensive tripods and more robust (and expensive) systems custom built at HVO (Orr and Hoblitt, 2008) and mounted on heavy surveying tripods. The built-in light sensor on the Wingscapes® cameras, meant to turn the cameras off at night, was removed to allow continuous photography. The time-lapse images from both system types provided start times for some breakouts and offered a unique look at tube-roof uplift in a few instances. Both systems recorded images only on-site, requiring frequent visits to exchange camera memory cards. The Wingscapes® cameras required regular exchange of internal batteries; the batteries for the HVO-constructed cameras were charged via a small solar panel. Image sizes varied from 1600 × 1200 to 3264 × 2448, depending on deployment.

3. Tumulus geometry measurements

3.1 Digital Elevation Models

Accurate topographic measurements of the sinuous tumulus, such as by using kinematic GPS, were not made during the tumulus's development due to insufficient field time. However, a Digital Elevation Model (DEM) of the distal part of the tumulus was created well after emplacement from oblique aerial photographs using the Agisoft® Photoscan Professional software package. The aerial photographs were captured from helicopter in July 2014 with a Canon EOS 60D digital SLR camera (18 megapixel image resolution). Photo registration is based on targets (white crosses) visible within the photographs and located by kinematic GPS (vertical and horizontal accuracy empirically determined to be ~5 cm). Target heights were transformed from ellipsoidal coordinates to orthometric coordinates using the National Geodetic Survey GEOID12a model. The horizontal and vertical accuracy of the resulting DEM is estimated at 10 cm.

The pre-eruption surface was taken from a June 2006 Federal Emergency Management Agency (FEMA) coastal LiDAR survey with a horizontal accuracy of 30 cm and a vertical accuracy of 14 cm. The LiDAR data were transformed into a DEM using ArcGIS 10.1, which was also used to perform DEM calculations and differencing between pre- and post-emplacement surfaces.

3.2 Crack and tumulus measurements

The width and depth of the axial (or dominant) crack on or near the crest of the sinuous tumulus were measured using a metal carpenter's tape at 20 locations along the part of the tumulus still exposed in 2014. The crack width was measured between piercing points; the crack depth that was measured is a minimum because the metal tab at the end of the tape prevented full insertion into the crack, as did roughness and rubble at the base of the crack. ArcGIS 10.1 was used to measure the width of the tumulus at each location from a rectified aerial image mosaic created using Agisoft® Photoscan Professional.

4. Description of eruptive activity

4.1 Eruptive setting and historical overview

Kīlauea's eruptive activity has been dominated since 1983 by effusion from vents within the volcano's East Rift Zone during a single prolonged eruptive sequence—the Puʻu ʻŌʻō eruption (Fig. 1) (e.g., Heliker and Mattox, 2003; Orr et al., in press). This activity is fed ultimately by basaltic magma thought to rise from depths of 60 to 90 km in the mantle (e.g., Eaton and Murata, 1960; Wright, 1984; Wyllie, 1988; Sen and Jones, 1990) and collects within storage reservoirs ~1–5 km beneath Kīlauea's summit (e.g., Fiske and Kinoshita, 1969; Ryan, 1987). From the summit, magma is transported ~20 km through the volcano's East Rift Zone at a depth of ~3 km (e.g., Klein et al, 1987; Montgomery-Brown et al. 2010; Lundgren et al., 2013) to the eruption site.

During its first 3 years, the eruption was dominated by episodes of lava fountaining that built the Puʻu ʻŌʻō pyroclastic cone (Wolfe et al., 1988; Heliker and Mattox, 2003; Heliker et al., 2003). Since 1986, however, the eruption has been characterized by nearly continuous effusion from a series of vents at and near Puʻu ʻŌʻō (Mattox et al., 1993; Mangan et al., 1995; Heliker et al., 1998; Kauahikaua et al., 1996; Heliker and Mattox, 2003; Orr et al., in press). This includes six years of effusion from the Kupaianaha vent 3 km northeast of Puʻu ʻŌʻō (1986–1992), 15 years of effusion from a succession of vents on the southwest flank of Puʻu ʻŌʻō (1992–2007), four years of effusion from the "episode 58" vent between Puʻu ʻŌʻō and Kupaianaha (2007–2011), two years of effusion from a vent on the northeast flank of Puʻu ʻŌʻō (2011–2013), one year of effusion from a vent within Puʻu ʻŌʻō (2013–2014), and most recently by effusion from a vent on the northeast flank of Puʻu ʻŌʻō (2014–ongoing). Several other short-lived (days-long) eruptions, from other nearby vents, also occurred during these periods. This study focuses on the eruptive activity that occurred from June to November 2010, while the episode 58 vent was active.

4.2 June–July 2010 eruptive activity

The lava tube transporting lava from the episode 58 vent to the Pacific Ocean ruptured at an elevation of ~600 m in early June 2010, and the new breakout captured the entire East Rift Zone eruptive output (Fig. 1). At first, the surface flow advanced slowly across gently sloping (2–3º) terrain near the breakout point, sequentially constructing six low rootless shields over the developing lava tube.

The front of the lava flow reached the upper slope of Pūlama Pali in early July, at the eastern end of the Hilina fault system that cuts Kīlauea's southeastern flank. Following the eastern margin of older episode 58 lava flows, the active flow gained speed and began traveling southward down the ~6º slope of Pūlama Pali. As it neared the base of the slope, the flow split into two branches—a more rapid western branch and a slower, broader eastern branch (Fig. 2). The western branch reached the base of the slope at an elevation of ~40 m on July 14. Blocked by older, inflated episode 58 flows to the south, the active flow turned sharply to the east, seeking the easiest path across the gently sloping (<2º) coastal plain (Fig. 2).

Traveling 400–500 m day^{-1}, the western branch of the flow advanced in a sheet-like fashion following the margin of an inflated flow (generally less than 2 m high) emplaced a few months earlier (Fig. 2a). The northern side of the advancing flow abutted a gentle slope (≤1º) with mostly small-scale (<1 m-high) flow features. Confined by low topography on both sides, the flow remained narrow (Fig. 2), rarely exceeding a width of 80 m. In a few places the entire flow was less than 30 m across. The flow thickness after its initial emplacement was ~1 m but locally may have been as much as 2 m along its axis. Assuming an average thickness of 1 m and the area of the coastal flow as mapped each day, we calculate

a bulk discharge for the advancing lobe of ~0.6 $m^3 s^{-1}$. The average void space fraction for the upper meter of the flow was measured after emplacement at 40%, which yields a dense rock equivalent (DRE) discharge that rounds to 0.4 $m^3 s^{-1}$. This is an order of magnitude less than Kīlauea's long-term East Rift Zone DRE discharge of ~4 $m^3 s^{-1}$ (converted from ~0.13 $km^3 yr^{-1}$; Sutton et al., 2003). Based on field observations, the discharge of the eastern branch appeared to be comparable to (or slightly less than) that of the western branch. Together, the eastern and western flow branches constituted the entire output from the episode 58 vent—the only active vent. This calculation implies that the East Rift Zone eruptive output at that time was ~1 $m^3 s^{-1}$, or roughly a quarter of the long-term rate.

On July 17, the flow reached a low (~6-m-high), south-facing embankment, on the southern side of State Highway 130 (Fig. 2), and spilled down into a shallow graben bounded to the south by the Hākuma horst. The flow moved slowly eastward, filling the graben and destroying one home while threatening others in Kalapana Gardens. This same subdivision was inundated previously by lava in 1990 (Mattox et al., 1993), and about 30 houses had since been built—or rebuilt—upon the 1990 lava flows. On July 25, lava topped the Hākuma horst and flowed into the ocean. The flow's eastward advancement stopped within a few days, having reached within ~50 m of two other homes.

We calculate the volume of lava accumulated within the graben between July 17 and July 25 by subtracting the underlying topography from the new flow surface, assumed to form a level plain with an elevation of 15 m (the elevation of the Hākuma horst at the point where it was topped). Flows emplaced outside the bounds of the graben during this period were assumed to have a thickness of 1 m, based on field observations, and a time span of 192 hours was used (mapping was completed on both days at about 1100 HST). Using these values yields a bulk discharge of ~0.7 $m^3 s^{-1}$ and a DRE discharge that rounds to 0.4 $m^3 s^{-1}$, consistent with our earlier calculation.

A relatively well-developed lava tube had formed as early as July 26, establishing a subsurface connection between the episode 58 vent and the Pacific Ocean (Fig. 1). Part of the tube's path, extending ~1.5 km from the buried trace of Highway 130 to the base of Pūlama Pali, was well expressed by a distinct line of fume easily followed on the ground. The lava tube approximately followed the centerline of the flow and crudely traced the shape of the older underlying episode 58 flow margin through much of this zone. Over the following ~10 days, lava from the eastern flow branch crossed and buried most of the lava tube within ~0.5 km of the base of the slope.

4.3 Sinuous tumulus formation and morphology

By late August 2010, the lava tube roof had begun to arch up in response to flow inflation. This formed a 1-km-long tumulus with a pronounced sinuosity (Fig. 3). The tumulus was a single continuous feature, not a series of adjacent or overlapping tumuli. Where the lava flow was very narrow, nearly its entire width was involved in the inflation, and in a few places one edge of the tumulus coincided with the edge of the flow. In one location, buried early in the study period, patches of the older flow ~20 m apart bounded both sides of the tumulus, showing that the entire width of the flow at that location had evolved into the tumulus.

The tumulus was covered by a network of cracks (the most pronounced sub-parallel to the trend of the tumulus) that appeared to have largely evolved from early-formed cooling joints (Figs. 3 and 4; Peck and Minakami, 1968; Hon et al., 1994; Rossi and Gudmundsson, 1996; Schaefer and Kattenhorn, 2004). As a result, the axial crack was not simply a single linear feature, but instead jogged sharply along its trend, especially where it adjusted to bends in the tumulus (Fig. 4a), and in some places was divided into sub-parallel en echelon segments (Fig. 4b). Where narrow, the tumulus was topped by a relatively

well-developed axial crack (Figs. 3 and 4a) that exposed textures indicative of inflation (Hon et al., 1994; Anderson et al., 1999). The axial crack widened and deepened as inflation progressed and the tumulus evolved, and was up to ~0.7 m wide and ~2.9 m deep after activity ceased (Table 1). In places where the tumulus was broad, the axial crack was much narrower or even non-existent, with flexure of the tumulus apparently accommodated by a few sub-parallel cracks (Fig. 4b).

The flanks of the tumulus expressed no significant inflation rifts as is seen on the sides of inflated sheet flows (Hon et al., 1994; Hoblitt et al., 2012). However, long cracks with minor vertical offset formed along the lower flanks of the tumulus in response to local breakouts. There was also no apparent vertical asymmetry in the growth history of the two flanks of the tumulus anywhere along its length (Anderson et al., 2012), nor did the axial crack contain lava squeeze-ups, as is often seen on other tumuli (Walker, 1991; Duraiswami et al., 2001; Anderson et al., 2012). The upslope end of the sinuous tumulus was buried early on by other flows, and the tumulus there emerged from beneath this younger cover, indicating that it extended farther upslope. Indeed, short sections of the tumulus farther upslope were visible through holes within this younger cover up to the base of Pūlama Pali. The terminus of the tumulus, roughly coincident with the buried trace of Highway 130, sloped down and merged with the surrounding flow surface in a fashion typical for tumuli (Walker, 1991; Rossi and Gudmundsson, 1996).

The tumulus stood up to ~4 m above the surrounding lava surface. This was, however, an apparent height because the flanks of the tumulus were partly inundated by breakouts from the tumulus itself (described below). Differencing of the pre- and post-emplacement surfaces show that the sinuous tumulus had a maximum height of nearly 8 m (Table 1).

Table 1. Table showing width and depth of dominant crack on or near crest of sinuous tumulus, width of exposed tumulus, tumulus height determined by differencing pre- and post-emplacement DEMs, and tumulus aspect (height/width) ratio at 20 locations spaced sub-equally along tumulus shown in Figure 4. Tumulus widths measured from rectified photo in direction approximately perpendicular to tube direction; crack width measured between piercing points; crack depth limited by depth to which metal carpenter's tape could be inserted.

Station	Crack width (m)	Crack depth (m)	Tumulus height (m)	Tumlus width (m)	Aspect ratio
1	0.32	1.5	5.6	9.7	0.58
2	0.30	2.9	5.5	13.5	0.41
3	0.72	1.6	5.6	9.4	0.60
4	0.55	1.9	4.8	11.2	0.43
5	0.33	1.6	4.6	13.5	0.34
6	0.41	1.9	5.1	12.1	0.42
7	0.59	1.7	5.0	7.0	0.71
8	0.40	1.9	5.6	10.7	0.52
9	0.31	2.2	5.6	10.6	0.53
10	0.55	1. 8	4.0	6.9	0.58
11	0.09	1.4	5.0	19.7	0.25
12	0.21	2.0	5.6	44.9	0.12
13	0.22	1.8	6.4	30.8	0.21
14	0.30	1.4	6.6	28.6	0.23
15	0.40	1.4	6.7	28.4	0.24
16	0.26	1.6	6.4	12.6	0.51
17	0.36	1.5	7.5	16.6	0.45
18	0.50	2.4	7.7	16.9	0.46
19	0.36	1.8	7.5	18.5	0.41
20	0.30	1.9	6.9	14.0	0.49

4.4 DI events and breakouts: August–November 2010

During 2010, cycles of deflation and inflation (DI events) at Kīlauea's summit (Fig. 5; Cervelli and Miklius, 2003; Poland et al., 2011), recorded across the summit tiltmeter network, deformed the edifice and caused variations in discharge from the episode 58 vent. Generally, within a few hours of the onset of summit deflation, a tiltmeter on the north flank of Puʻu ʻŌʻō likewise recorded the onset of deflation. This was followed, over the next day, by a decline in the abundance and vigor of surface flows as well as a pronounced diminution in the steam plume created by lava entering the ocean. These decreases in flow field activity were observed repeatedly and reductions in discharge are inferred to have accompanied all DI events.

Deflation at Kīlauea's summit switched invariably to rapid inflation, usually within a day or two (Fig. 5). After a few hours, Puʻu ʻŌʻō likewise began to inflate, and discharge from the episode 58 vent increased soon after that. In most cases, recovery of the magmatic system resulted in a surge in output from the vent, which commonly resulted in short-lived breakouts from points along the lava tube between the top of the Pūlama Pali and the ocean, where the carrying capacity of the tube was exceeded. In some instances, the delay between the onset of the inflation phase of a DI event and its related breakout was such that, by the time the breakout started, the deflation phase of the next DI event had already begun.

Starting in August 2010, breakouts driven by DI events began to occur repeatedly from the sinuous tumulus that extended ~1 km inland from the buried trace of Highway 130 (Figs. 3 and 6). In all, 22 breakouts occurred from various locations along the tumulus in our study area from August through November (Table 2; Figs. 5 and 6). In addition, several other breakouts associated with DI events occurred outside the study area, both upslope and downslope. Thirteen of the breakouts from the tumulus can be related directly to DI events, and five others accompanied a general increase in tilt during the second half of November, after the repeated DI events ceased temporarily (Fig. 5). The correlation between the remaining four breakouts and DI events is not obvious. Specifically, a breakout on October 9 followed several days without a DI event, and may have been related to the inflated condition of the volcano at that time. A breakout on October 12 began just a few hours after the start of the inflation phase of a DI event, but it may have been related to the earlier inflated condition of the volcano to which the October 9 breakout possibly responded. Two breakouts occurred several hours apart on October 15. Though both were probably related to the same DI event, the 17-hour delay between them makes the relation ambiguous. For this reason, only the earlier breakout is counted as being related to a DI event. Finally, a breakout on October 31 occurred just before the trough of a DI event. Because of the nearly 2-day delay between the onset of the previous inflation and the start of the breakout, the cause of the breakout is uncertain and it is not counted as being related to a DI event.

Table 2. Table showing start date and time for each sinuous tumulus breakout (precision in parentheses), dates and times that bracketed end time of breakouts, and final area of breakouts. Date and time also shown for onset of summit inflation for DI events associated with breakouts, except where noted. Final column shows delay between onset of summit inflation and onset of breakouts where applicable.

No.	Start Date/Time	End Date/Time (Bracketed)	Area (km^2)	DI Event Inflation Start	Delay (hours)
1	Aug 2, 0200 (±4 hr)	Aug 4, ~1330 – Aug 5, ~1030	0.028	Aug 1, 1004	15.9
2	Aug 16, 0300 (±15 min)	Aug 17, ~2000 – Aug 18, ~1000	0.033	Aug 14, 2248	28.2
3	Aug 18, 0300 (±5 hr)	Aug 18, ~1000 – Aug 19, ~1000	0.037	Aug 16, 1112	39.8
4	Aug 21, 1500 (±3 hr)	Aug 22, 1000 – Aug 23, 1045	0.028	Aug 20, 1014	28.8
5	Sep 15, 1800 (±6 hr)	Sep 15, Night – Sep 16, Morning	0.009	Sep 14, 1814	23.8
6	Sep 26, 0445 (±5 min)	Sep 28, 1200 – Sep 28, 2000	0.043	Sep 25, 0844	20.0
7	Sep 30, 1430 (±1 hr)	Oct 4, 1200 – Oct 5, 1030	0.030	Sep 28, 1356	24.6

8	Oct 4, 1600 (±2.5 hr)	Oct 10, 1330 – Oct 11, 1100	0.039	Oct 3,1508	24.9
9	Oct 9, 1040 (±5 min)	Oct 11, 1400 – Oct 13, 1000	0.035	(no related DI event)	—
10	Oct 12, 0215 (±5 min)	Oct 13, 1200 – Oct 15, 1030	0.036	(uncertain relation)	—
11	Oct 15, 0045 (±5 min)	Oct 15, 1250 – Oct 16, 0830	0.004	Oct 14, 0553	18.9
12	Oct 15, 1740 (±30 min)	Oct 19, 1130 – Oct 20, 1300	0.066	(uncertain relation)	—
13	Oct 20, 1033 (±2 min)	Oct 21, 1530 – Oct 22, 1145	0.016	Oct 19, 1851	15.7
14	Oct 27, 0007 (±2 min)	Oct 28, 1100 – Oct 29, 1330	0.027	Oct 25, 2214	25.9
15	Oct 31, 1435 (±15 min)	Nov 1, 1400 – Nov 2, 1100	0.016	(uncertain relation)	—
16	Nov 1, 1839 (±2 min)	Nov 2, 1300 – Nov 2, 1800	0.007	Oct 31, 1810	24.5
17	Nov 6, 1646 (±5 min)	Nov 8, 0550 – Nov 8, 1800	0.013	Nov 5, 2053	19.9
18	Nov 15, 1314 (±2 min)	Nov 18, 1115 – Nov 19, 1030	0.028	(no related DI event)	—
19	Nov 17, 0555 (±1 min)	Nov 25, 1030 – Nov 27, 0930	0.076	(no related DI event)	—
20	Nov 20, 0458 (±1 min)	Nov 29, 1530 – Nov 30, 1000	0.162	(no related DI event)	—
21	Nov 24, 1642 (±2 min)	Nov 29, 1530 – Nov 30, 1000	0.143	(no related DI event)	—
22	Nov 26, 2018 (±1 min)	Nov 28, 1515 – Nov 29, 1000	0.017	(no related DI event)	—

Several of the breakouts were composed of multiple breakout points along the length of the sinuous tumulus and from both flanks (e.g., Aug 21 breakout; Fig. 6a). Many of these additional breakouts were small (hundreds of square meters or smaller), and we group all the individual breakouts associated with a particular event together. The areas of coverage shown in Table 2 reflect this. We suspected but were not able to confirm directly that, during instances when there were multiple breakout points from the sinuous tumulus during a single event, the breakout point farthest upslope occurred first, suggesting a pulse of lava traveling through the tube and causing breakouts progressively downslope as the pulse advanced. This was certainly the case in a broader sense, with breakouts upslope, on Pūlama Pali, starting before breakouts on the coastal plain. That this also occurred on a smaller scale is supported by the fact that the breakout point farthest downslope (when there were multiple breakouts along the sinuous tumulus) was always the most voluminous and longest lived. Had it opened first, the other breakouts upslope would probably not have occurred. We were not able to determine the volume of each breakout, but the area covered by each breakout might be an adequate proxy for comparing the relative sizes of the breakouts because all breakouts were erupted onto similar terrain. However, the area covered by each breakout from the tumulus within our study cannot be used to gauge the size of the pulse of lava traveling through the tube system because other breakouts from the tube corresponding with DI events often occurred outside the study area.

The larger breakouts had a vigorous start, with lava usually flooding from the tube as a sheet for tens of minutes to a few hours. These starts were easy to spot if they were in view of the webcams or time-lapse cameras, and they were often observed (and start time noted) by Kalapana Gardens residents and sightseers. Thus, the start times of most of the breakouts are relatively well constrained, often to a few minutes (Table 2). The breakouts waned quickly (tens of minutes to a few hours), but weak activity—identified only because of our detailed daily mapping—sometimes continued for days. Because of this, the stagnation time of each breakout (Table 2) is poorly constrained, being bracketed by sequential field visits. Fig. 5 shows the timing of the breakouts and their estimated duration compared to the tilt record from station UWE, one of Kīlauea's summit tiltmeters.

The breakouts were sourced from cracks flanking the lower sides of the tumulus and widened the flow dramatically, burying the lower ground on both sides of the sinuous tumulus and slowly inundating it (Figs. 3, 4 and 7). Flow inflation, at least early on, caused progressive growth of the tumulus so that much of it remained a topographic high and was not buried by these subsequent breakouts (Fig. 3).The locations of these breakouts were not obviously related to the sinuosity of the tumulus (i.e., they did not

preferentially occur either at bends or along straight sections of the underlying lava tube). At the onset of the breakouts, the tube roof was abruptly and irrecoverably pushed up (Online Resource 1). This may be the dominant way in which the tube roof lifted after flow inflation seems to have stopped. Inelastic uplift likewise helped the tube roof remain higher than the slowly thickening (by burial) flow field on both sides. Both mechanisms (inflation and inelastic uplift) permitted much of the early-formed emplacement surface to remain uncovered while the surrounding terrain was repeatedly buried by breakouts.

Because growth of the tumulus over the tube was more rapid in some areas than in others, the height of the tumulus varied along its length so that elongate, dark-colored whaleback structures were formed (Figs. 3 and 4). The lower saddles between the whaleback structures were places that never hosted a breakout, and thus did not experience inelastic uplift. Some of the lows were eventually buried, subdividing what was originally a single long tumulus into an apparent chain of shorter tumuli (Fig. 4). The vertical evolution of the tumulus was not obviously related to its sinuosity, with higher parts of the tumulus just as likely to occur over straight sections as over bends in the tube.

Breakouts corresponding to the effusive surges caused by DI events occurred until mid-November. At that time, the DI events temporarily stopped happening, and the summit began a gradual inflationary trend. Along the studied section of the tube, this was manifested as a series of longer-lasting breakouts that covered correspondingly larger areas. Moreover, as many as three of these breakouts were active simultaneously, perhaps owing to an increase in discharge through the tube. Eventually, the tube upslope near the top of Pūlama Pali was unable to transmit the amount of lava it was carrying and, on November 29, it ruptured. The tube downslope from that point was abandoned thereafter, and the breakouts on the coastal plain subsequently stagnated. The November 29 breakout advanced downslope and eventually reached the coastal plain, where it buried most of the sinuous tumulus, leaving a few short segments partially exposed.

5. Discussion

5.1 Development of an inflated lava tube

Coastal flow emplacement during the Pu‘u ‘Ō‘ō eruption has generally followed a common pattern. The flows usually spread out upon reaching the gently sloped coastal plain, after traveling down the steeper slopes of Pūlama Pali, and advance by the progressive extension of pāhoehoe lobes (e.g., Peterson et al., 1994; Hon et al., 1994; Hoblitt et al., 2012). When fed at an eruption rate near or above the long-term average for the Pu‘u ‘Ō‘ō eruption, it usually takes one to three weeks for the leading tip of a flow to cross the coastal plain. Significant flow thickening via inflation and overplating occurs during this advance. On the other hand, when a flow is fed at an eruption rate well below the long-term average, or when a flow near or above the average rate is subdivided into smaller branches, the lava may stall on the hummocky surface of the coastal plain and make little forward progress. In such situations, it may take months before lava completely crosses the coastal plain, if it does so at all. In either case, once a flow tops the sea cliff, the inflating flow probably experiences a sudden drop in fluid pressure. Thereafter, the fluid core of the flow inland of the sea cliff chills quickly as lava is focused preferentially into the most energy efficient pathway between the base of Pūlama Pali and the ocean. Flow inflation and lateral spreading slow and stop, usually within a day or two, and a well-developed lava tube forms quickly.

The flow we studied during July–November 2010 evolved in a slightly different fashion, in that it was easily confined by low topography because of its low discharge. As a result, the flow failed to spread out and crossed the coastal plain quickly despite its relatively low flux. Little inflation occurred before the

flow poured over the low embankment on the south side of Highway 130. This embankment provided the same sort of topographic break that the sea cliff affords in other circumstances. Because of the inferred drop in fluid pressure, lava beneath the surface crust of the flow upslope from Highway 130 became concentrated along the thickest part of the flow. Thus, flow advance and lava tube formation occurred more rapidly than is typical for low discharge flows at Kīlauea and did not involve significant lateral spreading. Initial inflation across the entire width of the flow was minimal, and the flow failed to resurface itself as it usually does during flow emplacement through pāhoehoe lobe extension (Peterson et al., 1994). Morphologically, the flow had a relatively flat surface characteristic of sheet flows (Hon et al., 1994). The section of the lava tube between the base of Pūlama Pali and the Highway 130 embankment was, in a sense, isolated, and it evolved somewhat independently from other parts of the tube.

The inflation that occurred subsequently was focused along the axis of the incipient lava tube, which, when it began to form, was correspondingly thinner than the total thickness of the flow and probably had with a wide, elliptical cross-section (Kauahikaua et al., 1998). Conduction of heat through the roof, floor, and sides of the tube caused crustal growth and thickening. The subsequent corresponding pressure increase within the tube, due to decreasing cross-sectional area without a decrease in flow rate, forced the tube roof to arch up (Fig. 7; Hon et al., 1994; Kauahikaua et al., 1998). The result was a low, but well-defined, sinuous tumulus above the axis of the lava tube that meandered as a continuous feature across the coastal plain for a distance of ~1 km (Fig. 3). The height of the sinuous tumulus was further enhanced by irrecoverable uplift caused by the many breakouts from its flanks.

Peterson et al. (1994) describe another process by which an arched tube roof can form—accretion of lava onto levees during channelized flow. If the channel is sufficiently narrow these levees can grow together, forming an arched roof over the channel. While morphologically similar, the formation process is different from that which we describe, and the tube roof that forms in each case should be easily distinguishable in the field setting.

Inflation was possible only while the tube was completely full and lava was in contact with the tube roof. The depth of the axial crack on top of the tube gives an estimate of the time elapsed to develop a crust of that thickness. The empirical formula of Hon et al. (1994),

$$t = 164.8\ C^2 \qquad (1)$$

where t is time in hours and C is crustal thickness in meters, yields a total duration of ~57 days to form a 2.9-m-thick crust. The flow on the coastal plain at the measurement location, however, was active for a total of ~137 days, suggesting that the lava stream was in contact with the tube ceiling slightly less than half the time. Keszthelyi (2012) modified the formula of Hon et al. (1994) to better account for emplacement and environmental conditions appropriate for Kīlauea's south coast. Using the Keszthelyi (2012) formula,

$$t = 323.5\ C^2 \qquad (2)$$

yields a duration of ~113 days for formation of a 2.9-m-thick crust. This result indicates that the lava stream was in contact with the tube ceiling most of the time. Regardless, both results suggest periods during which head space separated the lava stream and tube ceiling.

The sinuous tumulus we describe does not fit into any tumulus classification scheme defined previously, though it is most similar to the flow-lobe tumuli of Walker (1991) and Rossi and Gudmunsson (1996). Walker (1991) and Rossi and Gudmunsson (1996) classify flow-lobe tumuli by height/width and

width/length aspect ratios. However, partial burial of the flanks of the sinuous tumulus by its own breakouts, combined with the extreme length and sinuosity of the tumulus, prevent a meaningful comparison with these parameters. For example, Rossi and Gudmunsson (1996) found that the flow-lobe tumuli that they measured had an average aspect ratio of 0.17 ± 0.06, while we find the aspect ratio of the sinuous tumulus varies from 0.12 to 0.71, depending on where along the tumulus's length the measurement is made (Table 1, Fig. 4).

No relation has been established between axial crack width and other geometrical tumulus parameters. In general, though, the width of the axial crack in the sinuous tumulus (Table 1) is much narrower than the axial cracks in similarly sized flow-lobe tumuli as described by Walker (1991) and Rossi and Gudmunsson (1996). This is consistent with our model that the sinuous tumulus was formed in part by inelastic uplift of the lava tube roof during breakouts, when the tube was overfilled by increased flux, and not entirely by inflation.

Anderson et al. (2012) found that some tumuli form over horizontal bends in the underlying flow pathways. Variations in height along the length of the sinuous tumulus we studied showed no obvious correspondence to bends in the tube. In our case, height variations reflect the presence or absence of breakouts—the lowest areas along the tumulus were those that experienced no breakouts and, thus, little or no inelastic uplift. What controlled the location of the breakouts along the tumulus, however, is not known, but may have been related to local variations in other factors, such as tube width, tube slope, or flow thickness.

5.2 Earth and Mars examples

Very long sinuous tumuli aligned with a lava tube, like that which we describe here, have not been described before from Hawai‘i, though they have been observed both before and since (authors' unpublished data). Very long tumuli, with no mention of sinuosity or tube relationship, are mentioned by Wentworth and Macdonald (1953), who call them "pressure ridges". However, they lump together ridge-like features formed by inflation as well as those formed by lateral compression. Hon et al. (1994) mention "long sinuous ridges" that form over blockages in major lava tubes, but provide no additional description. Cashman and Kauahikaua (1997) also mention "sinuous tumuli" forming over lava tubes, but likewise provide no additional description. The large tumulus they studied (the Woodchip tumulus) did form over a lava tube, but it was a single elongate whaleback structure, about 230 m long and weakly sinuous, that formed in a large sheet flow. Kauahikaua et al. (1998) describe "a train of inflating, elongate tumuli" that developed over a Pu‘u ‘Ō‘ō lava tube on the gently sloping coastal plain during 1996–1997. These tumuli were a source of breakouts during pulses of lava through the tube following eruptive pauses. The tumuli, however, were smaller and more equant than the tumulus we describe, though their positions followed the sinuous trace of the tube over which they developed (J. Kauahikaua, personal communication, 2013).

Glaze et al. (2005) describe a chain of very large tumuli on the 1843 flow from Mauna Loa (Hawai‘i). While those tumuli cluster along a linear trend, they are not shaped like the sinuous tumulus, and Glaze et al. (2005) found no evidence for a long-lived tube beneath the tumuli. Some elongate, crescent-shaped tumuli are present on the coastal plain portion of the 1859 Mauna Loa flow (F. Trusdell, personal communication, 2013), but they are no more than about 100 m in length. Their relation to a tube system is not known, and they are not mentioned by Walker (2009) who conducted a detailed study of tumuli and lava rises in the same area. Chitwood (1994) describes inflated lava fields in central and southeast Oregon, USA, and indicates that long narrow tumuli can form over lava tubes but provides no

discussion of tumuli dimensions and points to no specific examples. Finally, the Undara lava field in north Queensland, Australia, contains a 40-km-long sinuous inflation ridge ("The Wall"; Atkinson et al., 1975; Stephenson et al., 1998) which has been suggested as an analog for lunar rilles (Atkinson and Atkinson, 1995). This 200-m-wide, flat-topped feature has been demonstrated to be a narrow, inflated sheet flow (J. Kauahikaua, personal communication, 2013), much like similar inflation ridges on the much younger Toomba basalt flow of north Queensland, Australia (Whitehead and Stephenson, 1998).

Only a few sinuous tumuli like the one we observed forming in Hawai'i have been described world-wide. While many examples probably exist, the two we are aware of are found on the prehistoric Carrizozo and McCartys flows, New Mexico, USA. These are among the youngest and best preserved basaltic flow fields in the continental United States (Zimbelman and Johnston, 2002). The proximal and distal regions of both flows display evidence for flow inflation and were presumably linked by lava tubes (Keszthelyi and Pieri, 1993; Zimbelman and Johnston, 2001; 2002; Crumpler et al., 2007). The medial section of each flow is comparatively narrow due to confining topography and contains an elongate ridge that is, in some places, more than 10 m high. If the model presented here explains the formation of these ridges, then they are capped by lava emplaced early in each flow's history, and pāhoehoe flows that flank and partly inundate the ridges were sourced from the ridges themselves. Testing these expected relationships should help to determine if these sinuous ridges formed as described above, and will help constrain the emplacement conditions.

Sinuous ridges similar in size to those we identified in Hawai'i and New Mexico are observed within the plains flows of the Tharsis volcanic province of Mars (Fig. 8). Here, low shields and fissure vents erupted flows that coalesced to form a gently sloping plain. The sinuous ridges within the flows are up to 10 m in height and are the sources for small, local surface flows. Similar ridges found elsewhere across the surface of Mars have been interpreted as inverted fluvial channels (e.g., Burr et al., 2009; Williams et al., 2009; Burr et al., 2010; Zimbelman and Griffin, 2010; Lefort et al., 2012), eskers (Baker, 2001; Head and Pratt, 2001; Bleacher et al., 2003; Ghatan and Head, 2004; Banks et al., 2009), or eroded remnants of subsurface dikes (Head et al., 2006). The development of inverted fluvial channels and eskers involves flowing water, and all three of these proposed processes require significant erosion and regional deflation.

Although the plains units of the Tharsis region do not display obvious confining topography to drive localized tube-related inflation, lava flow thicknesses across Mars are suggested to be on the order of tens of meters (Keszthelyi et al., 2008; Mouginis-Mark and Rowland, 2008; Hamilton et al., 2010; Hamilton et al., 2011), comparable to the confining topography described above and sufficient to enable this process on Mars. The interpretation of sinuous ridges on Mars as elongate tumuli over lava tubes provides new insight into such ridges. While alternative (e.g., regional deflation or fluvial) hypotheses are viable for some martian sinuous ridges, the hypothesis that these features are inflated lava tubes is the most likely in volcanic terrains that do not show evidence of regional erosion. The tube formation processes described by Greeley (1987) and Peterson et al. (1994) may apply to flow fields on the flanks of much larger (hundreds of km in diameter) martian shield volcanoes (Bleacher et al., 2007a,b) where slopes are several degrees or higher and distinct ridges, as shown in Fig. 8, are not observed.

5.3 Forecasting lava tube breakouts

Forecasting volcanic activity is a driving motivation for volcano research and monitoring. Generally, forecasts for impending eruptive activity, especially the larger changes, improve as the time of the eruption approaches. During ongoing eruptive activity, though, there is a myriad of small changes that

occur with little or no warning. During August–November 2010, however, activity at Kīlauea behaved in such a way that we were able to forecast the occurrence, and to some extent the location and timing, of lava tube breakouts that threatened houses in the nearby Kalapana Gardens subdivision. This information was disseminated in daily volcanic activity updates on the HVO webpage and was transmitted directly to HCCD to improve their preparedness in the event that homes were threatened.

The correlation between the inflationary phase of DI events at Kīlauea's summit and the subsequent increase in eruptive activity along Kīlauea's East Rift Zone has been seen in hundreds of instances over more than a decade of observation, and the period discussed here was no exception. The occurrence of breakouts from the active tube system hours after the onset of summit inflation became apparent shortly after the flow was emplaced. It was not a perfect correlation with regard to our study area—33 DI events occurred from the beginning of August to mid-November, but only thirteen were associated with breakouts from the sinuous tumulus (Table 2). However, the DI events also often resulted in breakouts from other parts of the tube system, both upslope and downslope from the sinuous tumulus. Thus, those DI events that were not followed by breakouts from the sinuous tumulus were typically associated with breakouts elsewhere along the tube system. We also noticed that, on a few occasions (in particular September 30 and October 15), a coastal plain breakout spanned two DI events. In the September 30 case, the breakout waned quickly and was nearly inactive by October 2, but its activity had increased again by October 3, following another DI event. We infer the same for the October 15 case, though a gap in observation prevented confirmation. Finally, the effusive surge following some DI events, in particular those of the smallest magnitude, may have been completely accommodated by the tube system without a breakout.

Despite these shortcomings, our hazard assessments were predicated on the assumption that every DI event was capable of producing a breakout on the coastal flow field near Kalapana Gardens. The delay between the onset of the inflationary phase of the DI events and the start of the related breakouts ranged from 15.7 hours to 39.8 hours (Table 2), with an average delay of 23.9 hours. Our goal when communicating with Hawai‘i County Civil Defense authorities was to provide an assessment of potential activity for the following 24 hours. The delay between the inflation onset and subsequent breakouts fit well within this scheme.

Each breakout from the sinuous tumulus partly inundated the adjacent flank of the tumulus while leaving other sections unburied. Not surprisingly, we found that later breakouts were more likely to occur in areas that had not previously hosted a breakout, where the flank of the tumulus was not partly buried. With this in mind, we made a few attempts, with marginal success, to forecast the most likely points along the sinuous tumulus for the next breakout. Based on our visual inspection of the neighboring landscape, we could also make a rough estimate of the presumed flow direction for each of these potential breakout locations. However, there were simply too many spots along the tumulus from which breakouts could potentially occur for each DI event, and the breakouts did not always emerge from parts of the tumulus that were not covered, so we abandoned this part of our assessment. Moreover, because the distance from the tumulus to the nearest house was too great for breakouts to pose an immediate hazard, there was ample time once a breakout began to assess its probable flow path.

Destruction of Kalapana Gardens and neighboring communities in 1990 was controlled, in part, by eruptive pauses and subsequent restarts (Mattox et al., 1993). These pauses caused the flow that was active on the coastal plain to stall, and resumption of activity through the tube system resulted in new breakouts that followed the inflated margins of the existing flow (Mattox et al., 1993). Repeated breakouts led to flow field widening and further destruction. While modern tiltmeters like those

monitoring Kīlauea in 2010 were not in use at that time, other deformation tools showed a pattern of deflation and inflation similar to the DI events that caused variations in discharge in 2010. The 1990 events, however, were probably more akin to the "DID events" that occurred during 2000–2004 (Cervelli and Miklius, 2003; Poland et al., 2011). Regardless, the unsteady supply of lava through Kīlauea's East Rift Zone conduit, both in 1990 and in 2010, directly controlled the occurrence of lava tube breakouts near Kalapana, and these breakouts could be reliably forecast hours in advance using deformation data recorded at Kīlauea's summit.

6. Summary

Lateral confinement of a non-channelized basaltic lava flow by topography provides an important control on the flow's subsequent evolution. Rather than developing into a broad, inflated flow field, flow inflation may be focused directly over the tube, to form a long tumulus axial to the tube. The sinuous tumulus that we described here is one of a few examples known worldwide, and is the only one to have been observed throughout its formation. Its morphology and mechanism of formation was different than typical tumuli and, as such, it does not fit into any of the previously published tumuli classification schemes (Walker, 1991; Rossi and Gudmundsson, 1996). Its presence also shows conclusively that tumuli can form over major lava tube systems, a process questioned in the past (e.g., Walker, 1991).

Temporary increases in discharge pressurized the lava tube and caused inelastic uplift of the sinuous tumulus and breakouts from its flanks. The abrupt, forced uplift of the tube roof was in addition to flow inflation that occurred while the lava stream was in contact with the tube roof. The result was a sinuous tumulus composed of an early-formed lava surface surrounded by younger flows that emerged from the sides of the tumulus itself and buried the surrounding landscape. Eventually, low parts of the tumulus were buried by breakouts from adjacent areas of the tumulus itself. This subdivided the tumulus into a chain of shorter, elongate tumuli. We would not have known these were all part of a single, very long sinuous tumulus if we had not observed its entire evolution.

The ability of topography to confine a flow must be closely tied to the discharge. While all flows will be confined by sufficiently high topography, flows fed by progressively lower discharge can be confined by correspondingly lower topography, even down to the centimetric-scale (Hon et al., 1994; Rossi and Gudmundsson, 1996; Hamilton et al., 2013). We contend that the failure of the flow emplaced on Kīlauea's south flank during July–November 2010 to spread, thus causing its evolution into a sinuous, elongate tumulus, was controlled in part by its low discharge in this instance. A higher discharge, matching the long-term average at Kīlauea, would have likely resulted in a wider flow, more distributed inflation, and no tumulus above the axis of the tube that would have eventually formed. Sinuous tumuli found within narrow, topographically confined sections of the prehistoric McCartys and Carrizozo flows (New Mexico, USA) probably formed in an equivalent fashion, and we propose that these examples on Earth may be analogs for at least some sinuous ridges found within the Tharsis volcanic province and elsewhere on Mars.

Cycles of edifice deflation and inflation (DI events) at Kīlauea's summit cause decreases and increases in East Rift Zone output respectively. During the July–November 2010 study period, the decreases were manifested on the active flow field as diminutions in eruptive activity, while the increases led to breakouts from the active lava tube. As we described above, many of these breakouts came from the section of the lava tube topped by a ~1-km-long sinuous tumulus. Though imperfect, we used the

correlation between DI events and lava tube breakouts to forecast the possibility of new, potentially hazardous flows, which we communicated to Hawai‘i County Civil Defense.

Endorsement disclaimer

Any use of trade, product, or firm names herein is for descriptive purposes only and does not imply endorsement by the U.S. Government.

Acknowledgements

The authors would like to thank Christopher Hamilton, Laszlo Kestay, Don Swanson, Bruce Houghton, Sarah Fagents, and an anonymous reviewer, whose helpful comments improved this manuscript greatly. We thank Dave and Charlene Ewing for their willingness to host a webcam to assist with our monitoring of flow activity near Kalapana. Orr, Patrick, and Wooten were funded by the U.S. Geological Survey's Volcano Hazard Program. Funding for Bleacher was provided by NASA's Moon and Mars Analog Mission Activities Program.

References

Anderson, S.W., Stofan, E.R., Smrekar, S.E., Guest, J.E. and Wood, B., 1999. Pulsed inflation of pahoehoe lava flows: implications for flood basalt emplacement. Earth Planet. Sci. Lett., 168(1–2): 7–18.

Anderson, S.W., McColley, S.M., Fink, J.H. and Hudson, R.K., 2005. The development of fluid instabilities and preferred pathways in lava flow interiors: Insights from analog experiments and fractal analysis. Geological Society of America Special Papers, 396: 147–161.

Anderson, S.W., Smrekar, S.E. and Stofan, E.R., 2012. Tumulus development on lava flows: insights from observations of active tumuli and analysis of formation models. Bull. Volcanol. 74(4), 931–946.

Atkinson, A., Griffin, T.J. and Stephenson, P.J., 1975. A Major Lava Tube System from Undara Volcano, North Queensland. Bull. Volcanol. 39, 266–293.

Atkinson, A. and Atkinson, V.G., 1995. Undara Volcano and its tubes. Anne and Vernon Atkinson, Brisbane, Queensland.

Baker, V.R., 2001. Water and the martian landscape. Nature 412(6843), 228–236.

Banks, M.E., Lang, N.P., Kargel, J.S., McEwen, A.S., Baker, V.R., Grant, J.A., Pelletier, J.D. and Strom, R.G., 2009. An analysis of sinuous ridges in the southern Argyre Planitia, Mars using HiRISE and CTX images and MOLA data. J. Geophys. Res. 114(E9), E09003. doi:10.1029/2008JE003244.

Bleacher, J.E., Sakimoto, S.E.H., Garvin, J.B. and Wong, M., 2003. Deflation/erosion rates for the Parva Member, Dorsa Argentea Formation and implications for the south polar region of Mars. J. Geophys. Res. 108(E7), 5075. doi:10.1029/2001JE001535.

Bleacher, J.E., Greeley, R., Williams, D.A., Werner, S.C., Hauber, E. and Neukum, G., 2007a. Olympus Mons, Mars: Inferred changes in late Amazonian aged effusive activity from lava flow mapping

of Mars Express High Resolution Stereo Camera data, J. Geophys. Res. 112, E04003. doi:10.1029/2006JE002826.

Bleacher, J.E., Greeley, R., Williams, D.A., Cave, S.R. and Neukum, G., 2007b. Trends in effusive style at the Tharsis Montes, Mars, and implications for the development of the Tharsis province, J. Geophys. Res. 112, E09005. doi:10.1029/2006JE002873.

Burr, D.M., Williams, R.M.E., Wendell, K.D., Chojnacki, M. and Emery, J.P., 2010. Inverted fluvial features in the Aeolis/Zephyria Plana region, Mars: Formation mechanism and initial paleodischarge estimates. J. Geophys. Res. 115(E7), E07011. doi:10.1029/2009JE003496.

Burr, D.M., Bruno, B.C., Lanagan, P.D., Glaze, L.S., Jaeger, W.L., Soare, R.J., Wan Bun Tseung, J.-M., Skinner Jr., J.A. and Baloga, S.M., 2009. Mesoscale raised rim depressions (MRRDs) on Earth: A review of the characteristics, processes, and spatial distributions of analogs for Mars. Planet. Space Sci. 57, 579–596.

Cashman, K.J. and Kauahikaua, J.P., 1997. Reevaluation of vesicle distributions in basaltic lava flows. Geology 25(5), 419–422.

Cervelli, P.F. and Miklius, A., 2003. The shallow magmatic system of Kilauea volcano. In: Heliker, C., Swanson, D.A., Takahashi T.J. (Eds.), The Pu'u O'o - Kupaianaha Eruption of Kilauea Volcano, Hawaii: The First 20 Years. U.S. Geol. Surv. Prof. Pap. 1676, pp. 149–163.

Chitwood, L.A., 1994. Inflated basaltic lava—Examples of processes and landforms from central and southeast Oregon. Or. Geol. 56, 11–21.

Crumpler, L.S., Aubele, J.C. and Zimbelman, J.R., 2007. Volcanic features of New Mexico analogous to volcanic features on Mars. In: Chapman, M.G. (Ed.), The Geology of Mars: Evidence from Earth-Based Analog. Cambridge University Press, Cambridge, UK. ISBN-13 978-0-521-83292-2 (HB).

Duncan, A.M., Guest, J.E., Stofan, E.R., Anderson, S.W., Pinkerton, H. and Calvari, S., 2004. Development of tumuli in the medial portion of the 1983 aa flow-field, Mount Etna, Sicily. J. Volcanol. Geotherm. Res., 132(2–3): 173–187.

Duraiswami, R.A., Bondre, N.R., Dole, G., Phadnis, V.M. and Kale, V.S., 2001. Tumuli and associated features from the western Deccan Volcanic Province, India. Bull. Volcanol. 63(7), 435–442.

Du Toit, A.L., 1907. Pipe-amygdaloids. Geol. Mag. 43, 13–17.

Eaton, J.P. and Murata, K.J., 1960. How volcanoes grow. Science 132(3432), 925–938.

Fiske, R.S. and Kinoshita, W.T., 1969. Inflation of Kilauea Volcano prior to its 1967–1968 eruption. Science 165(3891), 341–349.

Glaze, L.S., Anderson, S.W., Stofan, E.R., Baloga, S. and Smrekar, S.E., 2005. Statistical distribution of tumuli on pahoehoe flow surfaces: Analysis of examples in Hawaii and Iceland and potential applications to lava flows on Mars. J. Geophys. Res. Solid Earth 110(B8), B08202. doi:10.1029/2004JB003564.

Ghatan, G.J. and Head, J.W., III, 2004. Regional drainage of meltwater beneath a Hesperian-aged south circumpolar ice sheet on Mars. J. Geophys. Res. 109(E7), E07006. doi:10.1029/2003JE002196.

672 Greeley, R., 1987. The role of lava tubes in Hawaiian volcanoes. In: Decker, R.W., Wright, T.L., Stauffer,
673 P.H. (Eds.), Volcanism in Hawaii. U.S. Geol. Surv. Prof. Pap. 1350(2), pp. 1589–1602.

674 Hamilton, C.W., Fagents, S.A. and Wilson, L., 2010. Explosive lava–water interactions in Elysium
675 Planitia, Mars: constraints on the formation of the Tartarus Colles cone groups. J. Geophys. Res.
676 115, E09006. doi:10.1029/2009JE003546.

677 Hamilton, C.W., Fagents, S.A. and Thordarson, T., 2011. Lava–ground ice interactions in Elysium
678 Planitia, Mars: geomorphological and geospatial analysis of the Tartarus Colles cone groups. J.
679 Geophys. Res. 116, E03004. doi:10.1029/2010JE003657.

680 Hamilton, C., Glaze, L., James, M. and Baloga, S., 2013. Topographic and stochastic influences on
681 pāhoehoe lava lobe emplacement. Bull. Volcanol., 75(11): 1–16. doi:10.1007/s00445-013-0756-
682 8.

683 Head, J.W., Wilson, L., Dickson, J. and Neukum, G., 2006. The Huygens-Hellas giant dike system on
684 Mars: Implications for Late Noachian–Early Hesperian volcanic resurfacing and climatic
685 evolution. Geology 34(4), 285–288.

686 Head, J.W., III and Pratt, S., 2001. Extensive Hesperian-aged south polar ice sheet on Mars: Evidence for
687 massive melting and retreat, and lateral flow and ponding of meltwater. J. Geophys. Res.
688 106(E6), 12275–12299. doi:10.1029/2000JE001359.

689 Heliker, C. and Mattox, T.N., 2003. The first two decades of the Pu‘u ‘Ō‘ō–Kupaianaha eruption;
690 chronology and selected bibliography. In: Heliker, C., Swanson, D.A., Takahashi, T.J. (Eds.), The
691 Pu‘u ‘Ō‘ō - Kupaianaha eruption of Kīlauea Volcano, Hawai‘i: The first 20 years. U.S. Geol.
692 Surv. Prof. Pap. 1676, pp. 1–27.

693 Heliker, C., Kauahikaua, J., Sherrod, D.R., Lisowski, M. and Cervelli, P., 2003. The rise and fall of Pu‘u
694 ‘Ō‘ō cone, 1983–2002. In: Heliker, C., Swanson, D.A., Takahashi, T.J. (Eds.), The Pu‘u ‘Ō‘ō -
695 Kupaianaha eruption of Kīlauea Volcano, Hawai‘i: The first 20 years. U.S. Geol. Surv. Prof. Pap.
696 1676, pp. 29–51.

697 Heliker, C.C., Mangan, M.T., Mattox, T.N., Kauahikaua, J.P. and Helz, R.T., 1998. The character of
698 long-term eruptions: inferences from episodes 50–53 of the Pu‘u ‘Ō‘ō - Kūpaianaha eruption of
699 Kīlauea Volcano. Bull. Volcanol. 59(6), 381–393.

700 Hoblitt, R.P., Orr, T.R., Heliker, C., Denlinger, R.P., Hon, K. and Cervelli, P.F., 2012. Inflation rates,
701 rifts, and bands in a pāhoehoe sheet flow. Geosphere 8(1), 179–195.

702 Hon, K., Kauahikaua, J., Denlinger, R. and Mackay, K., 1994. Emplacement and inflation of pahoehoe
703 sheet flows: observations and measurements of active lava flows on Kilauea Volcano, Hawaii.
704 Geol. Soc. Amer. Bull. 106(3), 351–370.

705 Kauahikaua, J., Mangan, M., Heliker, C. and Mattox, T., 1996. A quantitative look at the demise of a
706 basaltic vent: the death of Kupaianaha, Kilauea Volcano, Hawai‘i. Bull. Volcanol. 57(8), 641–
707 648.

708 Kauahikaua, J., Cashman, K.V., Mattox, T.N., Heliker, C.C., Hon, K.A., Mangan, M.T. and Thornber,
709 C.R., 1998. Observations on basaltic lava streams in tubes from Kilauea Volcano, island of
710 Hawaii. J. Geophys. Res. 103(B11), 27303–27323. doi:10.1029/97JB03576.

711 Keszthelyi, L., 2012. Rate of solidification of silicate melts on the Earth, Moon, Mars, and beyond. Proc.
712 43rd Lunar Planet. Sci. Conf., Cont. #1659, Woodlands, Texas, 19–23 Mar.

713 Keszthelyi, L., Jaeger, W., McEwe, A., Tornabene, L., Beyer, R.A., Dundas, C. and Milazzo, M., 2008.
714 High Resolution Imaging Science Experiment (HiRISE) images of volcanic terrains from the first
715 6 months of the Mars Reconnaissance Orbiter Primary Science Phase. J. Geophys. Res. 113,
716 E04005. doi:10.1029/2007JE002968.

717 Keszthelyi, L.P. and Pieri, D.C., 1993. Emplacement of the 75-km-long Carrizozo lava flow field, south-
718 central New Mexico. J. Volcanol. Geotherm. Res. 59(1-2), 59–75.

719 Klein, F.W., Koyanagi, R.Y., Nakata, J.S. and Tanigawa, W.R., 1987. The seismicity of Kilauea's magma
720 system. In: Decker, R.W., Wright, T.L., Stauffer, P.H. (Eds.), Volcanism in Hawaii. U.S. Geol.
721 Surv. Prof. Pap. 1350(2), 1019–1185.

722 Lefort, A., Burr, D.M., Beyer, R.A. and Howard, A.D., 2012. Inverted fluvial features in the Aeolis-
723 Zephyria Plana, western Medusae Fossae Formation, Mars: Evidence for post-formation
724 modification. J. Geophys. Res. 117(E3), E03007. doi:10.1029/2011JE004008.

725 Lundgren, P., Poland, M., Miklius, A., Orr, T., Yun, S.-H., Fielding, E., Liu, Z., Tanaka, A., Szeliga, W.,
726 Hensley, S. and Owen, S., 2013. Evolution of dike opening during the March 2011 Kamoamoa
727 fissure eruption, Kīlauea Volcano, Hawai`i. J. Geophys. Res. Solid Earth 118.
728 doi:10.1002/jgrb.50108.

729 Mangan, M.T., Heliker, C.C., Mattox, T.N., Kauahikaua, J.P. and Helz, R.T., 1995. Episode 49 of the
730 Pu‘u ‘O‘o–Kupaianaha eruption of Kilauea volcano – breakdown of a steady-state eruptive era.
731 Bull. Volcanol. 57(2), 127–135.

732 Mattox, T.N., Heliker, C., Kauahikaua, J. and Hon, K., 1993. Development of the 1990 Kalapana flow
733 field, Kilauea Volcano, Hawaii. Bull. Volcanol. 55(6), 407–413.

734 Montgomery-Brown, E.K., Sinnett, D.K., Poland, M., Segall, P., Orr, T., Zebker, H. and Miklius, A.,
735 2010. Geodetic evidence for en echelon dike emplacement and concurrent slow slip during the
736 June 2007 intrusion and eruption at Kīlauea volcano, Hawaii. J. Geophys. Res. 115(B7).
737 doi:10.1029/2009JB006658.

738 Mouginis-Mark, P.J. and Rowland, S.K., 2008. Lava flows at Arsia Mons, Mars: Insights from a graben
739 imaged by HiRISE. Icarus 198. doi:10.1016/j.icarus.2008.06.015.

740 Nichols, R.L., 1939. Surficial banding and shark's-tooth projections in the cracks of basaltic lava. Am. J.
741 Sci. 237, 188–194.

742 Orr, T.R., Poland, M.P., Patrick, M.R., Thelen, W.A., Sutton, J., Elias, T., Thornber, C.T., Parcheta, C.,
743 and Wooten, K.M., (in press). Kīlauea's 5–9 March 2011 Kamoamoa fissure eruption and its
744 relation to 30+ years of activity from Pu‘u ‘Ō‘ō, in Carey, R. J. et al. (eds.), Hawaiian volcanoes,
745 from source to surface, AGU Monograph 208.

746 Orr, T.R., 2011. Selected time-lapse movies of the East Rift Zone eruption of Kīlauea Volcano, 2004–
747 2008. U.S. Geol. Surv. Data Ser. 621, 15 p., 26 time-lapse movies.

748 Orr, T.R. and Hoblitt, R.P., 2008. A versatile time-lapse camera system developed by the Hawaiian
749 Volcano Observatory for use at Kīlauea Volcano, Hawai‘i. U.S. Geol. Surv. Sci. Invest. Rept.
750 2008-5117. 8 p.

751 Paskievitch, J., Read, C. and Parker, T., 2010. Remote telemetered and time-lapse cameras at Augustine
752 Volcano. In: Power, J.A., Coombs, M.L., Freymueller, J.T. (Eds.), The 2006 eruption of
753 Augustine Volcano, Alaska. U.S. Geol. Surv. Prof. Pap. 1769, pp. 285–293.

754 Peck, D.L. and Minakami, T., 1968. The Formation of Columnar Joints in the Upper Part of Kilauean
755 Lava Lakes, Hawaii. Geol. Soc. Amer. Bull., 79(9): 1151-1166.

756 Peterson, D.W., Holcomb, R.T., Tilling, R.I. and Christiansen, R.L., 1994. Development of lava tubes in
757 the light of observations at Mauna Ulu, Kilauea Volcano, Hawaii. Bull. Volcanol. 56(5), 343–
758 360.

759 Philpotts, A.R. and Lewis, C.L., 1987. Pipe vesicles—An alternate model for their origin. Geology
760 15(10), 971–974.

761 Poland, M.P., Miklius, A., Lundgren, P. and Sutton, A.J., 2011. Repeated deflation-inflation events at
762 Kilauea Volcano, Hawai'i: What's up (and down) with that? Abs. #V51G-01, 2011 Fall Meeting,
763 AGU, San Francisco, Calif., 5–9 Dec.

764 Poland, M.P., Dzurisin, D., LaHusen, R.G., Major, J.J., Lapcewich, D., Endo, E.T., Gooding, D.J.,
765 Schilling, S.P. and Janda, C.G., 2008. Remote camera observations of lava dome growth at
766 Mount St. Helens, Washington, October 2004 to February 2006. In: Sherrod, D.R., Scott, W.E.,
767 Stauffer, P.H. (Eds.), A Volcano Rekindled: The Renewed Eruption of Mount St. Helens, 2004–
768 2006. U.S. Geol. Surv. Prof. Pap. 1750, 225–236.

769 Rossi, M.J. and Gudmundsson, A., 1996. The morphology and formation of flow-lobe tumuli on Icelandic
770 shield volcanoes. J. Volcanol. Geotherm. Res., 72(3–4): 291–308.

771 Ryan, M.P., 1987. Neutral buoyancy and the mechanical evolution of magmatic systems. In: Mysen, B.O.
772 (Ed.), Magmatic Processes: Physiochemical Principles. The Geochemical Soc., pp. 259–287.

773 Schaefer, C.J. and Kattenhorn, S.A., 2004. Characterization and evolution of fractures in low-volume
774 pahoehoe lava flows, eastern Snake River Plain, Idaho. Geol. Soc. Amer. Bull., 116(3-4): 322–
775 336.

776 Schmincke, H.-U., 1967. Flow directions in Columbia River Basalt flow and paleocurrents of interbedded
777 sedimentary rocks, south-central Washington. Geol. Rundschau. 56, 992–1020.

778 Self, S., Keszthelyi, L. and Thordarson, T., 1998. The importance of pāhoehoe. Annu. Rev. of Earth and
779 Planet. Sci. 26(1), 81–110.

780 Sen, G. and Jones, R.E., 1990. Cumulate Xenolith in Oahu, Hawaii: Implications for Deep Magma
781 Chambers and Hawaiian Volcanism. Science 249(4973), 1154–1157.

782 Stephenson, P.J., Burch-Johnston, A.T., Stanton, D. and Whitehead, P.W., 1998. Three long lava flows in
783 north Queensland. J. Geophys. Res. 103(B11), 27359–27370. doi:10.1029/98JB01670.

784 Sutton, A.J., Elias, T. and Kauahikaua, J., 2003. Lava-effusion rates for the Pu‘u ‘Ō‘ō - Kupaianaha
785 eruption derived from SO_2 emissions and very low frequency (VLF) measurements. In: Heliker,

C., Swanson, D.A., Takahashi, T.J. (Eds.), The Pu‘u ‘Ō‘ō - Kupaianaha eruption of Kīlauea Volcano, Hawai‘i: The first 20 years. U.S. Geol. Surv. Prof. Pap. 1676, pp. 137–148.

Thornber, C.R., 1997. HVO/RVTS-1; a prototype remote video telemetry system for monitoring the Kilauea East Rift Zone eruption, 1997. U.S. Geol. Surv. Open-File Rep. 97-537, 18 p.

Walker, G.P.L., 1991. Structure, and origin by injection of lava under surface crust, of tumuli, “lava rises”, “lava-rise pits”, and “lava-inflation clefts” in Hawaii. Bull. Volcanol. 53(7), 546–558.

Walker, G.P.L., 2009. The endogenous growth of pahoehoe lava lobes and morphology of lava-rise edges. In: Thordarson, T., Self, S., Larsen, G., Rowland, S.K., Hoskuldsson, A. (Eds.), Studies in volcanology—the legacy of George Walker (Special Publications of IAVCEI No. 2). The Geol. Soc., pp. 17–32.

Wentworth, C.K. and Macdonald, G.A., 1953. Structures and forms of basaltic rocks in Hawaii. U.S. Geol. Surv. Bull. 994, 98 p.

Whitehead, P.W. and Stephenson, P.J., 1998. Lava rise ridges of the Toomba basalt flow, north Queensland, Australia. J. Geophys. Res. Solid Earth 103(B11), 27371–27382. doi:10.1029/98JB00029.

Williams, K.E., Toon, O.B., Heldmann, J.L. and Mellon, M.T., 2009. Ancient melting of mid-latitude snowpacks on Mars as a water source for gullies. Icarus 200(2), 418–425.

Wolfe, E.W., Neal, C.A., Banks, N.G. and Duggan, T.J., 1988. Geologic observations and chronology of eruptive events. In: Wolfe, E.W. (Ed.), The Puu Oo eruption of Kilauea Volcano, Hawaii; episodes 1 through 20, January 3, 1983, through June 8, 1984. U.S. Geol. Surv. Prof. Pap. 1463, 1–97.

Wright, T.L., 1984. Origin of Hawaiian Tholeiite: A Metasomatic Model. J. Geophys. Res. 89(B5), 3233–3252.

Wyllie, P.J., 1988. Solidus Curves, Mantle Plumes, and Magma Generation Beneath Hawaii. J. Geophys. Res. 93(B5), 4171–4181. doi:10.1029/JB093iB05p04171.

Zimbelman, J.R. and Johnston, A.K., 2002. New Precision Topographic Measurements of Carrizozo and McCartys Basalt Flows, New Mexico. In: Lueth, V.W., Giles, K.A., Lucas, S.G., Kues, B.S., Myers, R.G., Ulmer-Scholle, D.S. (Eds.), Geology of White Sands. N. M. Geol. Soc. Guideb., 53rd Field Conf., pp. 121–127.

Zimbelman, J.R. and Griffin, L.J., 2010. HiRISE images of yardangs and sinuous ridges in the lower member of the Medusae Fossae Formation, Mars. Icarus, 205(1), 198–210.

Zimbelman, J.R. and Johnston, A.K., 2001. Improved Topography of the Carrizozo Lava Flow: Implications for Emplacement Conditions. In: Crumpler, L.S., Lucas, S.G. (Eds.), Volcanology in New Mexico. N.M. Mus. Nat. Hist. Sci. Bull. 18, 31–136.

Fig. 1. Map showing extent of flows erupted from Kīlauea's East Rift Zone since 1983 (one small flow erupted in 2007 falls outside area shown here). Brown, flows erupted from 1983 to 2007. Yellow, episode 58 flow erupted 2007–2010. Red, phase of episode 58 flow described here, erupted June–November 2010. Dashed black line, active lava tube. Black open circles, rootless shields (not to scale) constructed over tube in June 2010. Contour interval, 50 m. Box shows map area for Fig. 6. (Inset) Island of Hawai'i and its five volcanoes. Dashed black lines, Kīlauea's rift zones.

Fig. 2. Infrared images (uniformly transparent) overlaid onto simultaneous visible-wavelength photographs showing flow advancement across coastal plain. Warmer colors indicate higher temperatures; areas of bright yellow to white, active or very recently active flows. (a) Abrupt eastward turn in flow direction at base of Pūlama Pali on July 14, 2010. White dotted line, active flow margin. Flow surface at lower left with mottled violet coloration, previously emplaced episode 58 flows. Dashed white line, trace of lava tube formed later. (b) Flow butted against Hākuma horst and filling in adjacent graben on July 23, 2010. White dotted line, active flow margin. White arrow, study area at narrow part of flow. White circles, houses labeled in Fig. 6a. House 1 destroyed July 25.

Fig. 3. Photographs of sinuous tumulus in study area. (a) October 19, 2010, photograph showing distant perspective of sinuous tumulus. Dashed white line, lava tube trace; arrowhead denotes flow direction. Partly transparent white line, buried trace of Highway 130. White boxes, approximate area of coverage of b and f. Dark lava surface along and adjacent to tube trace, early-formed lava surface emplaced July 2010. Lighter-colored lava surfaces, younger tube breakouts. (b) October 14, 2010, photograph of sinuous tumulus. Dashed white line, approximate trace of lava tube beyond ends of pronounced tumulus. Three most recent breakouts prior to October 14 labeled. White box, approximate coverage area of c, d, e, and g. (c) August 23, 2010, photograph and (d) November 16, 2010, photograph demonstrating inflation and tumulus uplift. White arrows, same point in photographs c and d. (e) October 5, 2010, photograph showing NE flank of sinuous tumulus. Movie in Online Resource 1 captured by time-lapse camera at right. September 30 breakout in foreground. Photograph by WB Garry, NASA. (f) August 23, 2010, photograph showing ~4-m-high tumulus in contact with underlying 1986–1992 lava surface. Note tiny breakout which leaked through tumulus side ~3 m above base on August 18. (g) October 1, 2010, photograph showing breakouts from flank cracks (dashed white lines; arrows show breakout flow direction) parallel to tumulus trend. Exposed tumulus ~2.5 m high. Note August 21 breakout surface not buried by September 30 breakout.

Fig. 4. (a–b) Rectified aerial image mosaics showing part of sinuous tumulus (outlined with dotted yellow lines) and related breakouts (demarkated by dashed yellow lines; labeled with start date) in study area. Numbered locations correspond to measurements recorded in Table 1. Flow direction in tube from left to right.

Fig. 5. Plot showing onset times for breakouts from sinuous tumulus (red lines) compared to DI events and other tilt changes recorded by tiltmeter (UWE) at Kīlauea's summit (black line). Gray boxes, approximate breakout durations. Darker gray shows where boxes overlap, indicating multiple active breakouts.

Fig. 6. Maps showing breakouts from sinuous tumulus. Pacific Ocean at lower right; Kalapana Gardens subdivision at upper right. Heavy red line, State Highway 130; thin red line, main entrance road into Kalapana Gardens; brown, flows emplaced 1986–1992; yellow, older episode 58 flows; light gray, lava from active flow emplaced July 15–31, 2010; white, areas not covered by lava (forested); light red, lava emplaced in July and early August 2010 (eastern branch of active flow), which originated farther upslope and buried part of active tube; dotted yellow line, trace of active lava tube; heavy black lines, normal faults that define Hākuma horst and adjacent graben (ball–bar symbols on down-dropped side); black squares, houses shown in Fig. 2b. (a–e) Final extent of various tube breakouts shown with different colors and labeled by start date. Lava tube (dotted yellow line) shown on top to highlight breakout source location. Dark gray area in each successive map b–e shows area covered by breakouts shown in previous panel. (f) Dark gray, composite of all tube breakouts erupted in study area August 1–November 30, 2010. Lava tube

shown beneath breakout composite to highlight tumulus where lava surface not reburied after emplacement. Breakouts on lava delta at lower right not shown. Dotted black lines, bounds of sinuous tumulus studied.

Fig. 7. Cartoon showing idealized cross-section through lava flow at different development stages. (a) Time step 1: Shortly after emplacment; well-developed tube not yet formed and inflation is minimal. (b) Time step 2: Tube has developed and tumulus has begun to form; pressurization of tube has resulted in breakout from tumulus flank. (c) Time step 3: Tumulus has undergone additional growth; breakouts, no longer active, have emerged from both flanks of tumulus, partly inundating it; head space has formed between lava stream and tube ceiling. (d) Time step 4: 3D perspective of tumulus showing active breakouts from several places along tumulus flanks in response to re-pressurization of lava tube.

Fig. 8. Images of sinuous ridges within Tharsis volcanic province of Mars. (a) Mars Reconnaissance Orbiter (MRO) Context (CTX) Camera image P07_003673_1774 (NASA/JPL-Caltech/MSSS) showing ≤10-m-high ridge (Solar Incidence Angle 53°; Sun ~ 37° above horizon). Arrow points to one example of small breakout sourced from ridge, but many are visible. (b) MRO High Resolution Imaging Science Experiment (HiRISE) Camera image ESP_027289_1790 (NASA/JPL/University of Arizona) showing low shield volcano in Tharsis plains (caldera at upper left; Solar Incidence Angle 54°; Sun ~36° above horizon) with two sinuous ridges that appear to be source of small surface flows. In both cases, ridge morphology appears where slopes decrease to <0.5º on lower flank of volcano.

Online Resource 1. Time-lapse movie showing abrupt uplift of sinuous tumulus (i.e., tube roof) correlated with October 9, 2010 breakout. Breakout emerged from lower flank of tumulus directly to right of camera, but traveled away from camera. Flow appears in camera view several hours later, after time period shown by movie. Camera capture interval is one image per minute; movie playback speed is 6 frames per second. Final movie frame shows lava tube trace and flow direction.

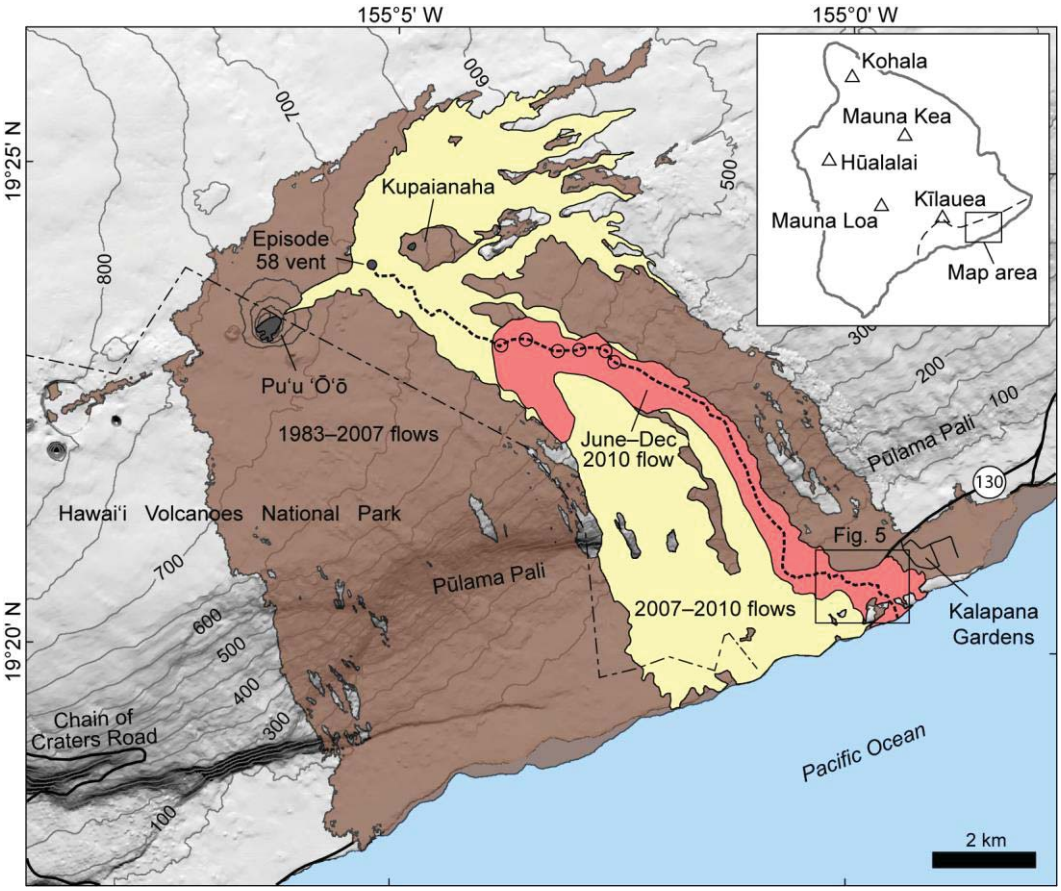
155°5' W
155°0' W
19°25' N
19°20' N
Kohala
Mauna Kea
Hūalalai
Mauna Loa
Kīlauea
Map area
Kupaianaha
Episode
58 vent
Pu'u 'Ō'ō
1983–2007 flows
June–Dec
2010 flow
Pūlama Pali
Hawai'i Volcanoes National Park
Fig. 5
2007–2010 flows
Kalapana
Gardens
Chain of
Craters Road
Pacific Ocean
2 km
600
700
800
500
400
300
200
100
130

887

888 Fig. 1

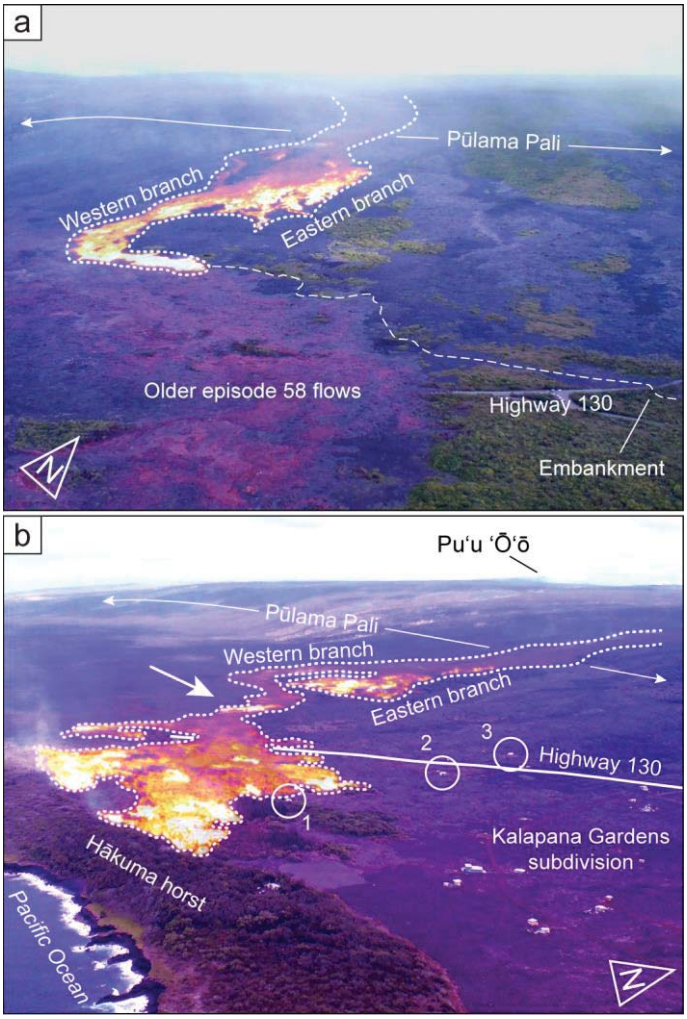
a
Pūlama Pali
Western branch
Eastern branch
Older episode 58 flows
Highway 130
Embankment
N
b
Pu'u 'Ō'ō
Pūlama Pali
Western branch
Eastern branch
2
3
Highway 130
1
Kalapana Gardens
subdivision
Hākuma horst
Pacific Ocean
N

889

890 Fig. 2

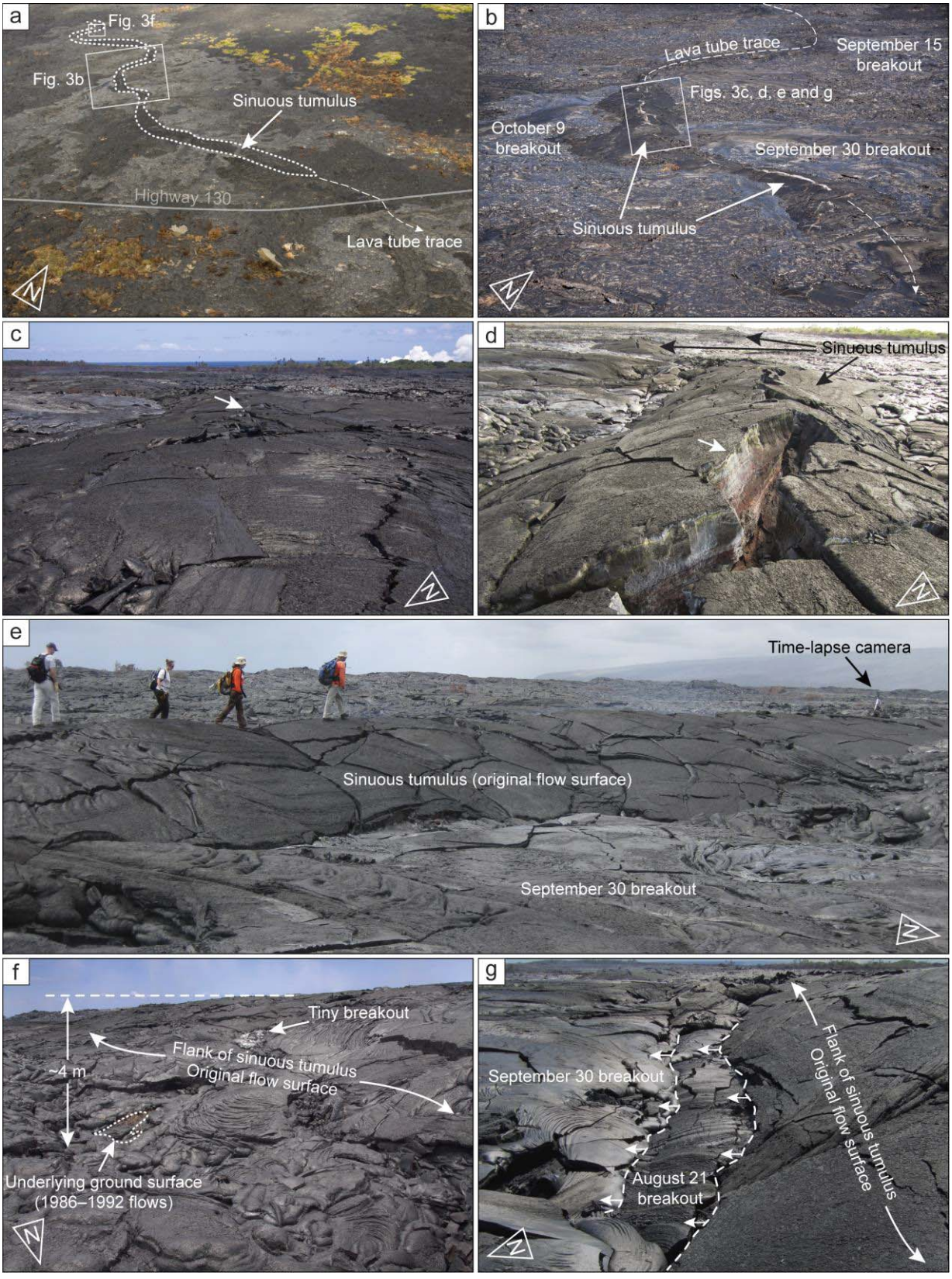
a
Fig. 3f
Fig. 3b
Sinuous tumulus
Highway 130
Lava tube trace
b
Lava tube trace
September 15 breakout
Figs. 3c, d, e and g
October 9 breakout
September 30 breakout
Sinuous tumulus
c
d
Sinuous tumulus
e
Time-lapse camera
Sinuous tumulus (original flow surface)
September 30 breakout
f
Tiny breakout
Flank of sinuous tumulus
Original flow surface
~4 m
Underlying ground surface
(1986–1992 flows)
g
September 30 breakout
Flank of sinuous tumulus
Original flow surface
August 21 breakout

891

892 Fig. 3

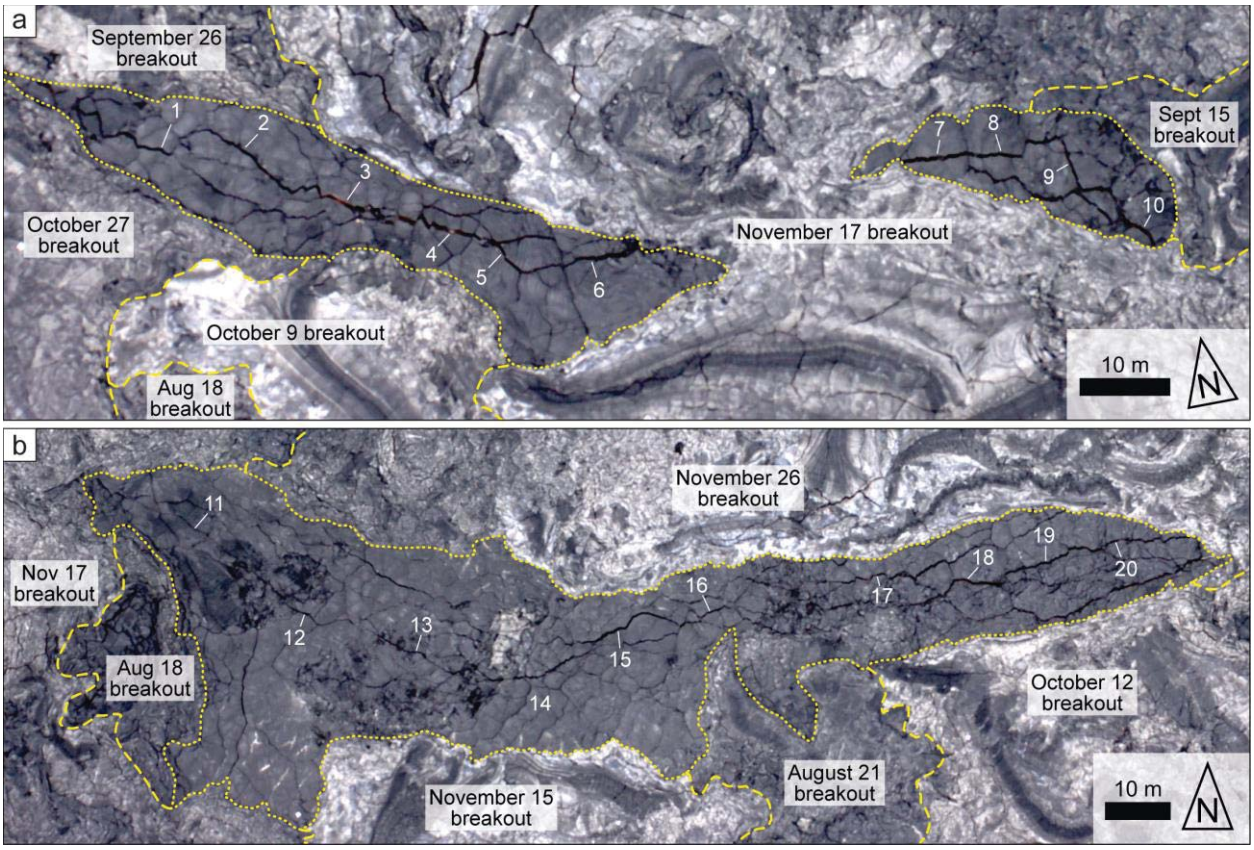

893

894 Fig. 4

895

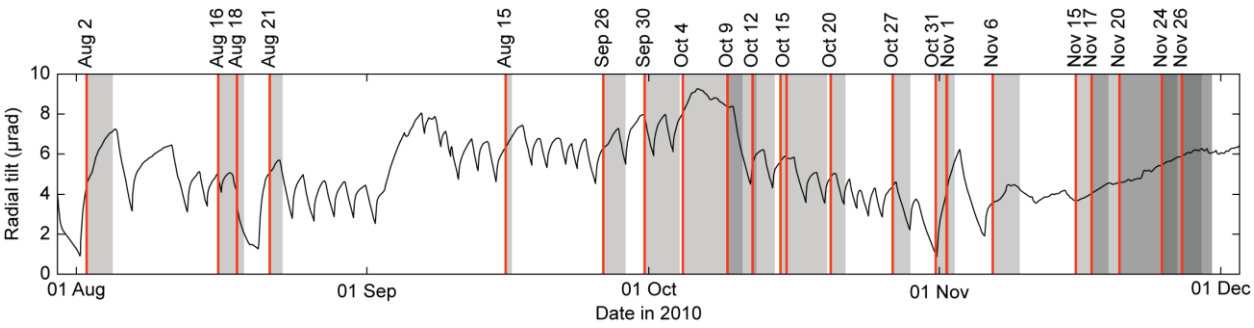

896

897 Fig. 5

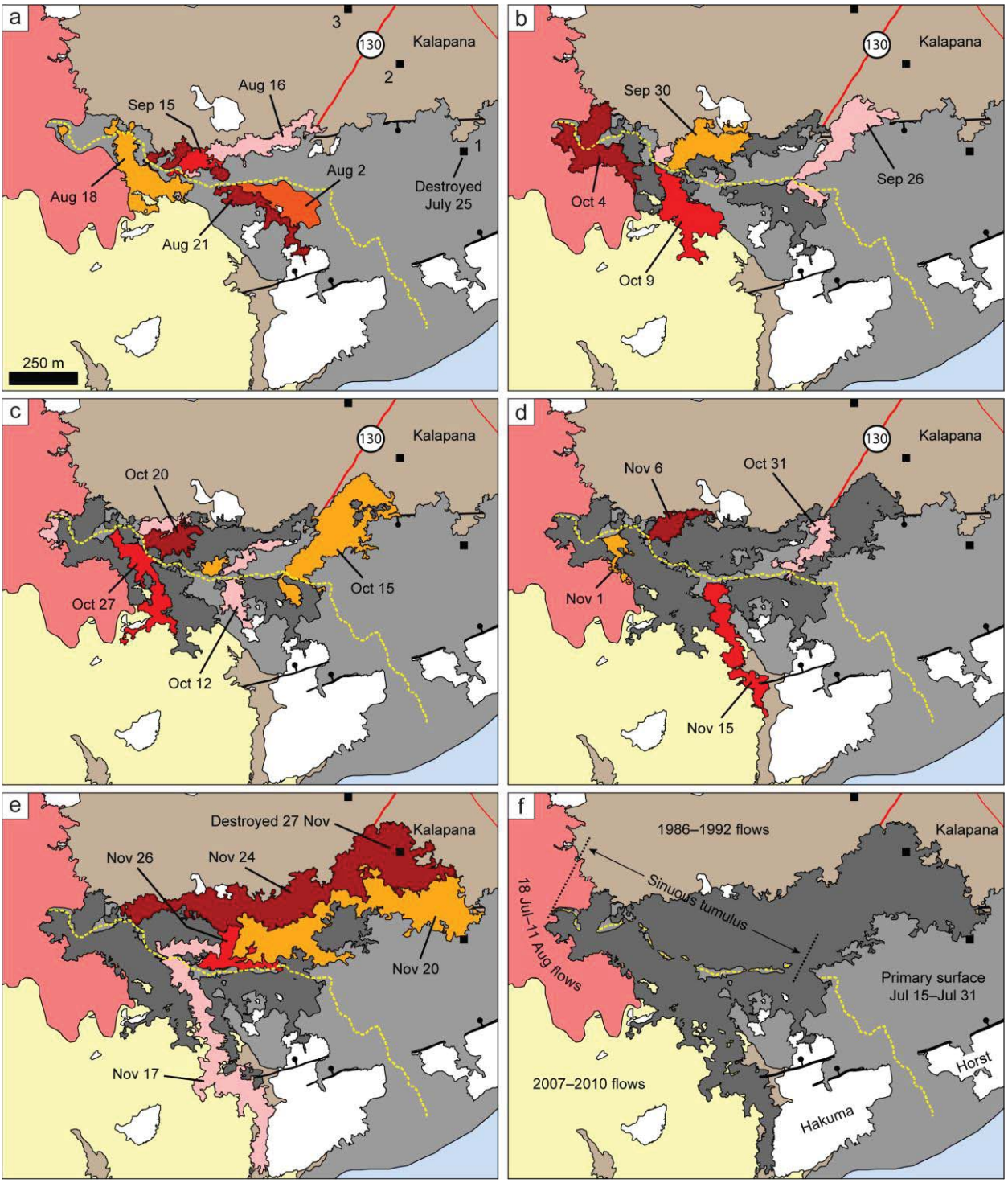

898

899 Fig. 6

900

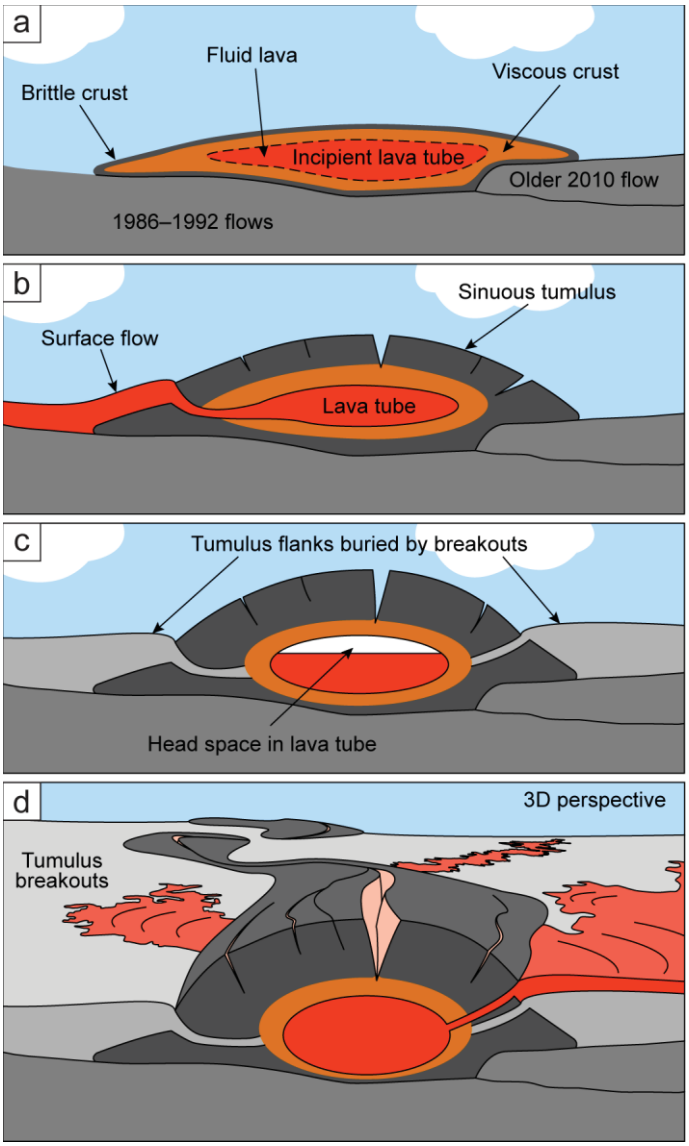
a
Fluid lava
Brittle crust
Viscous crust
Incipient lava tube
Older 2010 flow
1986–1992 flows
b
Sinuous tumulus
Surface flow
Lava tube
c
Tumulus flanks buried by breakouts
Head space in lava tube
d
3D perspective
Tumulus
breakouts

Fig. 7

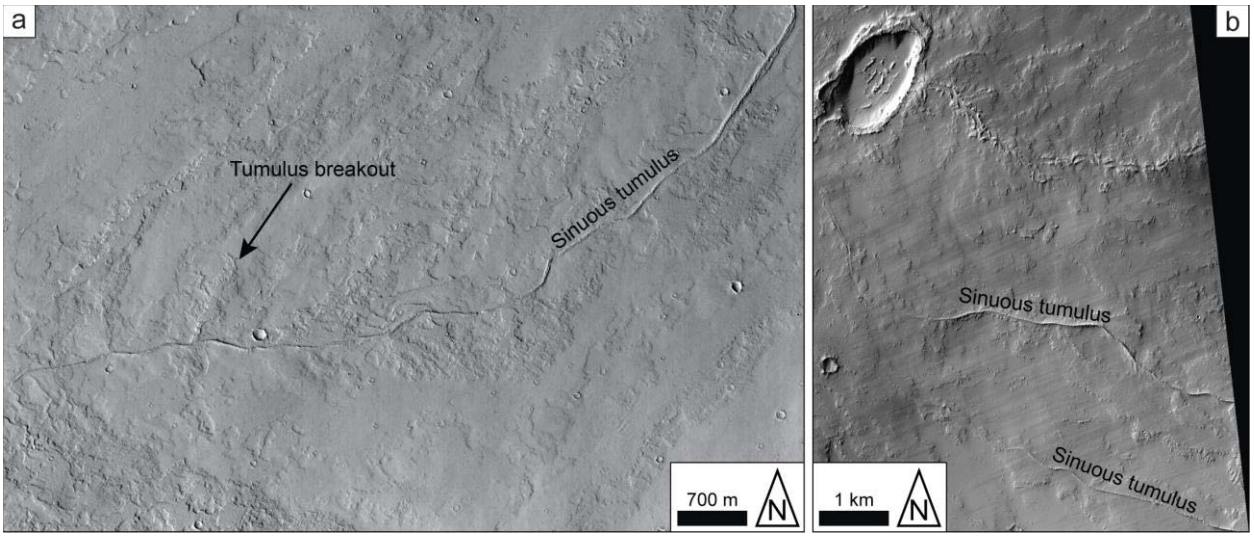
a
Tumulus breakout
Sinuous tumulus
700 m
N
b
Sinuous tumulus
Sinuous tumulus
1 km
N

Fig. 8